Volume 6 | Number 5 | 7 March 2016 | Pages 1237–1556

Catalysis Science & Technology

www.rsc.org/catalysis

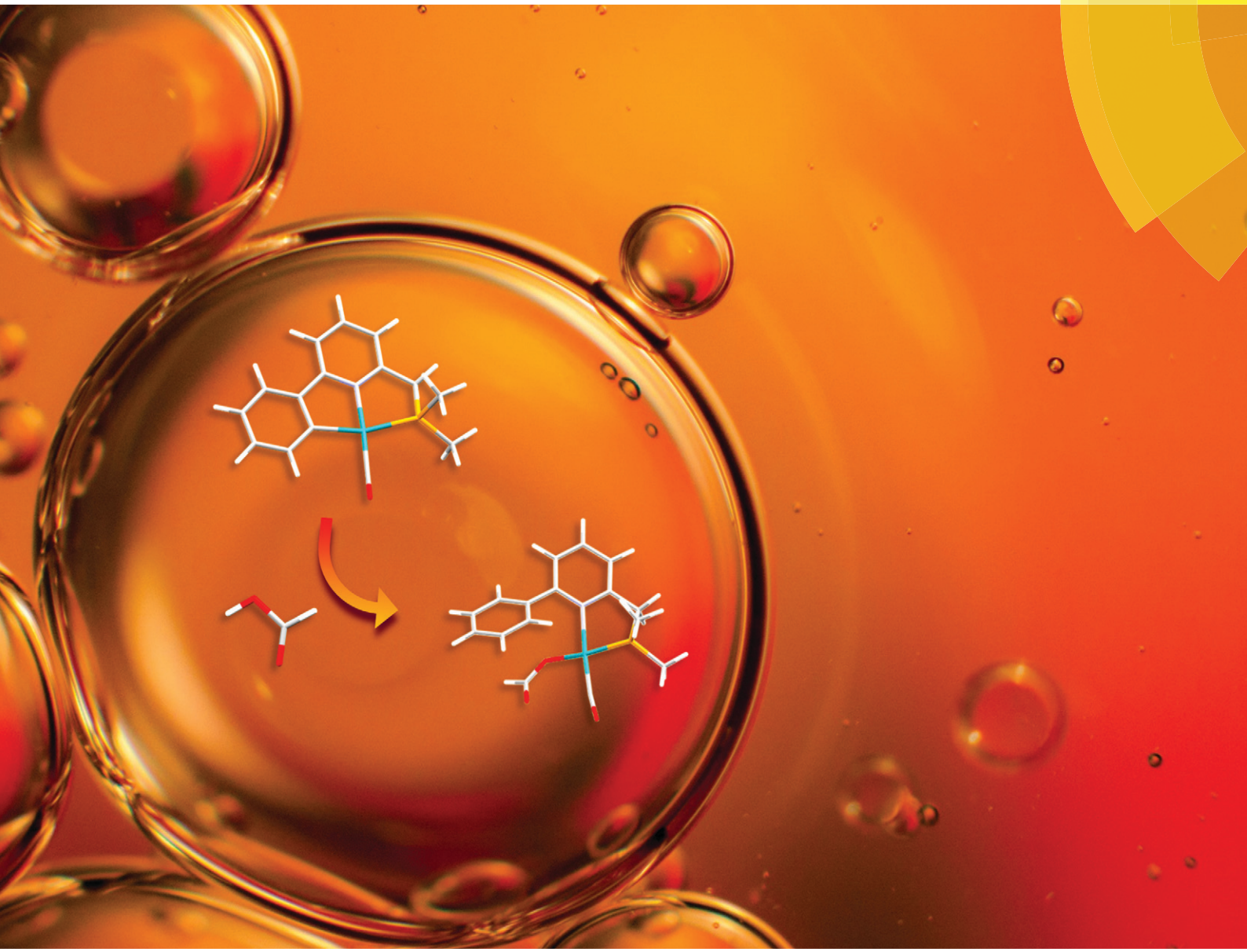

ISSN 2044-4753

ROYAL SOCIETY OF CHEMISTRY

PAPER

J. I. van der Vlugt *et al.*

Reversible cyclometalation at Rh^{I} as a motif for metal–ligand bifunctional bond activation and base-free formic acid dehydrogenation

175 YEARS

Catalysis Science & Technology

PAPER

View Article Online
View Journal | View Issue

Cite this: *Catal. Sci. Technol.*, 2016, **6**, 1320

Reversible cyclometalation at Rh^I as a motif for metal–ligand bifunctional bond activation and base-free formic acid dehydrogenation†

L. S. Jongbloed,[a] B. de Bruin,[a] J. N. H. Reek,[a] M. Lutz[b] and J. I. van der Vlugt*[a]

Received 8th September 2015,
Accepted 2nd November 2015

DOI: 10.1039/c5cy01505g

www.rsc.org/catalysis

Reversible cyclometalation is demonstrated as a strategy for the activation of small protic molecules, with a proof-of-principle catalytic application in the dehydrogenation of formic acid in the absence of an exogenous base. The well-defined Rh^I complex Rh(CO)(**L**) **1**, bearing the reactive cyclometalated PN(C) ligand **L** (L^H = PNC^H = 2-di(*tert*-butylphosphinomethyl)-6-phenylpyridine), undergoes protonolysis of the Rh–C_{Ph} bond with weak protic reagents, such as thiols and trifluoromethanesulfonamide. This system also displays bifunctional metal–ligand protonolysis reactivity with formic acid and subsequent decarboxylation of the formate complex. Density functional theory (DFT) calculations show that H_2 evolution from putative Rh(CO)(H)(L^H) complex **A** is very facile, proposedly encompassing formal C–H oxidative addition at Rh to give **C** *via* agostic intermediate **B** and subsequent reductive elimination of H_2. Complex **1** is a catalytically competent species for base-free formic acid dehydrogenation, with the intermediacy of formate complex **4**. DFT calculations reveal accessible barriers for involvement of a flanking phenyl group for both initial activation of formic acid and release of H_2, supporting a cooperative pathway. Reversible C–H activation is thus a viable mechanism for metal–ligand bifunctional catalysis.

Introduction

The application of reactive ligands for metal–ligand bifunctional bond activation and subsequent cooperative catalysis receives much attention.[1] Among the different reactive ligand designs, systems bearing a proton-responsive group (showing reversible deprotonation activity) are particularly attractive and versatile. Generally, two strategies to incorporate such a fragment (an 'internal base') within the ligand structure that can easily activate substrates co-exist: i) a site in the coordination sphere of a metal center and ii) a site at a location not directly connected to the metal center (2nd coordination sphere). Well-known designs implementing the latter strategy operate *via* reversible dearomatization by deprotonation of functionalized picoline,[2] aminopyridine,[3] or pyridone fragments.[4] Regarding the strategy involving proton-responsive groups in the coordination sphere of a transition metal, reversible deprotonation of metal-bound functionalized amines[5] has been successfully applied in a variety of catalytic transformations.

Metal–carbon bonds are typically rather strong, but their bond energy can be influenced by *e.g.* strain or non-ideal orbital overlap, as present in cyclometalated species. Reversible cyclometalation at late transition metals using strong acids has been well-documented for stoichiometric scenarios,[6–8] but examples with low-valent metal ions such as Rh^I and applications of this type of reactivity in catalytic turnover are rare, to the best of our knowledge. Metal–ligand bifunctional catalysis by reversible cyclometalation has been postulated as a possible mechanism with a few systems (Fig. 1). Mashima *et al.* discussed this strategy for the dehydrogenative silylation of phenylpyridines catalyzed by a cyclometalated iridium complex.[9] A similar 'roll-over' mechanism was suggested for base-free transfer hydrogenation with a ruthenium catalyst.[10] The cooperativity of a cyclometalated fragment in the ligand structure has also been proposed, on the basis of

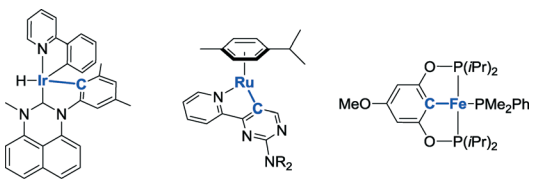

Fig. 1 Complexes that have been proposed to act as cooperative catalysts for different types of transformations *via* reversible cyclometalation.

[a] *Homogeneous, Bioinspired & Supramolecular Catalysis, van 't Hoff Institute for Molecular Sciences, University of Amsterdam, Science Park 904, 1098 XH Amsterdam, The Netherlands. E-mail: j.i.vandervlugt@uva.nl*
[b] *Crystal & Structural Chemistry, Bijvoet Center for Biomolecular Research, Utrecht University, Padualaan 8, 3584 CH, The Netherlands*

† Electronic supplementary information (ESI) available: Spectroscopic, crystallographic, catalytic and computational details. See DOI: 10.1039/c5cy01505g

computational studies, to be suitable for the dehydrogenation of ammonia-borane.[11–13] However, it was experimentally proven that this mechanism occurs most likely only in the early stage of catalysis[13] or as a way to generate an active species.[12]

Computational studies by Vanka *et al.* indicate that reversible cyclometalation can not only be useful for NH_3BH_3 dehydrogenation but can also be a suitable mechanism for formic acid dehydrogenation to CO_2 and H_2.[11] Dihydrogen is considered a key component of many future renewable energy solutions, but efficient and reversible storage and release of H_2, *e.g.* in organic liquids such as formic acid (FA), is essential for a hydrogen-based economy. Most catalytic systems for the dehydrogenation of HCOOH to H_2 and CO_2 require the presence of an exogenous base,[14] which not only decreases the overall hydrogen content from 4.4 wt% (for pure HCOOH) to 2.3 wt% (for a typical 5 : 2 HCOOH/NEt_3 mixture) but also necessitates post-catalysis processing for fuel cell applications (removal of volatile amines).[15] Hence, catalytic formic acid dehydrogenation should ideally be performed in the absence of such an exogenous base, but to date, only a limited number of systems capable of base-free formic acid dehydrogenation have been reported.[16]

Given our interest in the design of reactive ligand systems for cooperative bond activation reactions and catalytic processes,[17] we wondered whether reversible C–H activation in the coordination sphere of a metal could serve as a new methodology to facilitate *e.g.* formic acid dehydrogenation. In such a strategy, a metal–carbon fragment should function as an internal base for the activation of a suitable protic substrate. A hypothetical cooperative mechanism based on reversible cyclometalation as a bond-activation concept involves i) M–C bond-assisted E–H bond activation and ii) ligand-assisted Y–H bond reductive elimination after productive conversion of the activated M–E moiety into a product-like M–Y fragment (Scheme 1). Reversible cyclometalation by protonation of the M–C bond might result in a weakly coordinating agostic C–H bond.[18] This fragment could be viewed as masking a vacant site at the metal center, without significant perturbations (structural or electronic) of the global ligand framework, unlike what is often encountered for other reactive ligands. An agostic C–H interaction might also assist in stabilizing catalytically relevant intermediates, with beneficial implications for the overall energy profile of a potential reaction path.

Recently, we synthesized cyclometalated Rh^I complex **1** bearing the deprotonated derivative of ligand L^H that can act both as a neutral bidentate PN-ligand and as anionic tridentate PNC-system, depending on the reaction conditions.[19] Based on these initial results, we speculated that the ligand-based reactive carbon center in the coordination sphere of Rh^I could be employed as an internal base for the activation and conversion of functionalized protic substrates and that the flexidentate character of the ligand could be beneficial in catalysis. We previously studied the activation of alkynes,[20] activated amines[21] and thiols[22,23] using proton-responsive PN and PNP ligands coordinated to late transition metals using dearomatization/aromatization cooperativity. In this article, we describe the reactivity of the Rh–C bond toward related substrates and we report on the base-free dehydrogenation of formic acid as a proof-of-principle for the use of reversible cyclometalation in metal–ligand bifunctional catalysis.

Results and discussion

Reactivity of 1 toward weak protic donors – thiols

Cyclometalated complex **1** was shown to be susceptible to Rh–C cleavage by ethereal HBF_4 as a strong acid. This generates a Rh^I complex with an agostic Rh–(C_{Ph}–H) bond in the solid state, possibly *via* protonation of the metal to create a Rh^{III}(hydride) intermediate, with subsequent C–H reductive elimination. Furthermore, facile methylation at the cyclometalated carbon results from the reaction of **1** with MeI. Based on these initial results, the activation of less reactive substrates was investigated. Initial attempts to activate alcohols or phenylacetylene at r.t. did not result in Rh–C cleavage, based on NMR spectroscopy. This may point toward either a pK_a mismatch between these protic substrates and the metal–carbon bond as an 'internal base' or to unfavorable steric interference that prevents formal oxidative addition at the metal center.

Aliphatic thiols did react smoothly with **1**, judging from the rapid color change of the solution from red to light-yellow (Scheme 2). ^{31}P NMR spectroscopy was found to be very useful in monitoring the chemistry at the Rh–C bond *trans* to the phosphine donor. Hence, while **1** appears as a doublet at δ 76.31 ppm ($^1J_{Rh-P}$ = 101 Hz), the reaction with 1,3-propanedithiol led to a doublet at δ 69.75 ppm ($^1J_{Rh-P}$ = 151.7 Hz) for complex **2**. A strong IR-band for the carbonyl was present at ν 1938 cm^{-1} ($\Delta\nu$ of 5 cm^{-1} *vs.* **1**), while the

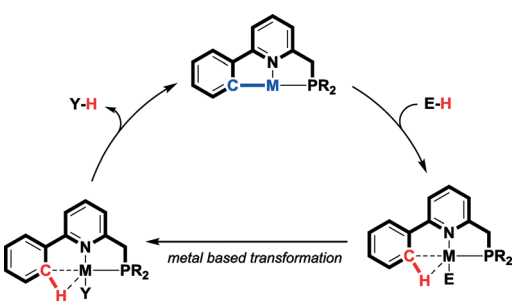

Scheme 1 Proposed pathway involving reversible cyclometalation for metal–ligand bifunctional bond activation and catalysis.

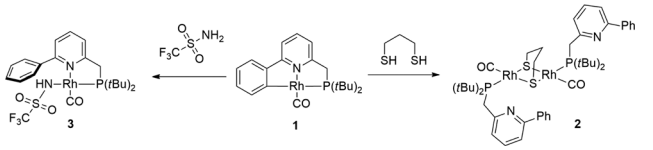

Scheme 2 Reactivity of Rh^I complex **1** toward 1,3-propanedithiol and trifluoromethanesulfonamide.

pyridine signals were significantly shifted downfield in the ^{1}H NMR spectrum. These data suggest the decoordination of the pyridine donor and thus the monodentate P-coordination of the PNC^H framework, induced by the tendency of the thiolate fragments to bridge metal centers. This hypothesis was corroborated by X-ray crystal structure determination of the single crystals of **2** grown from a concentrated acetone-d_6 solution (Fig. 2). The geometry around each Rh^I-center is square planar and the overall structural features with a *gem*-dithiolate core resemble those reported in the literature.[24]

Similar spectroscopic observations were made when **1** was allowed to react with benzyl mercaptan.[25] This behaviour is strikingly different from the chemistry observed for Ni-complexes with dearomatized tridentate PNP ligands,[22] although for Cu^I, this PNP scaffold was shown to adopt a dinucleating coordination mode.[23] Because of the decoordination of the pyridine from the metal, we did not pursue catalytic (hydro-addition) transformations involving thiols, as the proposed cooperative nature of reversible cyclometalation requires the proximity of the C–H bond to the metal, with the pyridine acting as directing group. Also, trifluoromethylsulfonamide reacts rapidly with the Rh–C bond (Scheme 2), which resulted in a ^{31}P shift for the resulting amide complex **3** at δ 103.7 ppm ($^1J_{Rh-P}$ = 152 Hz). The combined spectroscopic data are similar to the previously reported Pd(CH$_3$)(^{R}PN)(triflamide) species,[21] so coordination of the triflamide *trans* to phosphorus is proposed, although this compound could not be obtained as single crystalline material.

DFT calculations on H_2 activation with 1. Having demonstrated that cyclometalated Rh^I-system **1** is reactive toward (weakly) protic substrates, we sought to apply the concept of reversible cyclometalation in cooperative catalysis. Species **1** appeared stable under an H_2 atmosphere (20 bar) at r.t., indicating a relatively high barrier for heterolytic cleavage of H_2 to generate putative species **A**, Rh(H)(CO)(**1^H**). Heating an NMR sample for 1 hour at 70 °C under 35 bar of H_2 did not result in any observable hydride species. This 'inertness' toward heterolytic H_2 activation can be taken as an indication that the reverse reaction, *i.e.* H_2 evolution from **C** to generate **1**, may be a favourable pathway. To confirm this hypothesis, we performed DFT calculations (BP86, def2-TVZP, disp3 corrections) on monohydride complex **A** (Fig. 3). This species may convert, *via* agostic intermediate **B** and subsequent C$_{Ph}$–H oxidative addition, to dihydride **C** with a low barrier of 7.2 kcal mol^{-1}. This dihydride subsequently undergoes smooth reductive elimination of H_2 (6.9 kcal mol^{-1} barrier) to generate **1** as a stable product (ΔG = −7.6 kcal mol^{-1}). As a result, this cyclometalated complex may thus be a catalytically competent species for dehydrogenative reactions, which involve H_2 production.

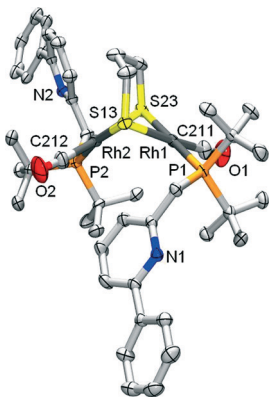

Fig. 2 ORTEP plot (50% displacement ellipsoids) for complex **2**. Selected bond lengths (Å) and angles (°): Rh$_1$–P$_1$ 2.3163(5); Rh$_1$–C$_{211}$ 1.827(2); Rh$_1$–S$_{13}$ 2.3940(5); Rh$_1$–S$_{23}$ 2.3784(5); Rh$_2$–P$_2$ 2.3154(6); Rh$_1$–C$_{212}$ 1.808(2); Rh$_2$–S$_{13}$ 2.3833(5); Rh$_2$–S$_{23}$ 2.3948(5); Rh$_1$···Rh$_2$ 3.0845(2); P$_1$–Rh$_1$–S$_{13}$ 94.682(18); S$_{13}$–Rh$_1$–S$_{23}$ 82.762(18); P$_2$–Rh$_2$–S$_{23}$ 93.690(19); S$_{13}$–Rh$_2$–S$_{23}$ 82.642(18). Angle sums Rh$_1$: 359.99(10); Rh$_2$: 360.44(12)°. Dihedral angle between S–Rh–S planes: 61.27(3)°.

Catalytic dehydrogenation of formic acid

To capitalize on the apparent facile loss of H_2 from putative species **A** in combination with the potential reactivity of the Rh–C bond in dehydrogenative catalysis and to illustrate the concept of reversible metalation for metal–ligand bifunctional substrate activation, we studied the dehydrogenation of formic acid as a proof-of-principle reaction. Addition of 20 molar equiv. of HCOOH to **1** in MeCN instantaneously resulted in a yellow complex that was characterized as formate derivative **4** (Scheme 3). Complex **4** (^{31}P: δ 105 ppm, $^1J_{Rh-P}$ 167 Hz) is the only species present at r.t., but upon warming to 55 °C in a closed NMR tube, deep-red species **1** is regenerated within 45 minutes. No trace of the remaining HCOOH was observed, and the formation of H_2 was detected (Fig. 4).

The use of HCOOD resulted in selective deuteration of both *ortho*-C–H groups on the phenyl ring in **1**, which is in line with the cooperative activation of FA over the Rh–C bond. No deuteration of the methylene spacer was observed under these conditions, as confirmed by ^{2}H NMR studies, excluding a role for this potentially reactive site during turnover. Smooth catalytic dehydrogenation of HCOOH was established using 0.5 mol% species **1** in dioxane at 75 °C, with a turnover frequency (TOF) of 169 mol mol^{-1} h^{-1} (see Fig. 5 and the ESI†). Addition of an external base (NEt$_3$) did not affect the catalytic activity.[26] Catalyst **1** showed reproducible performance during eight consecutive runs (a total TON

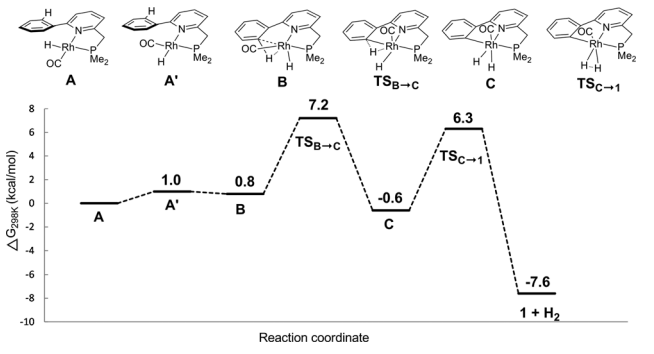

Fig. 3 DFT (BP86, def2-TZVP, disp3) calculated free energy profile (ΔG^0_{298K} in kcal mol^{-1}) of dihydrogen formation from hydride intermediate **A^{Me}**, with methyl instead of *tert*-butyl groups.

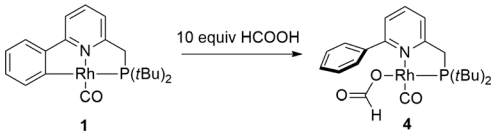

1 4

Scheme 3 Reactivity of Rh^{I} complex **1** toward 10 molar equiv. of HCOOH.

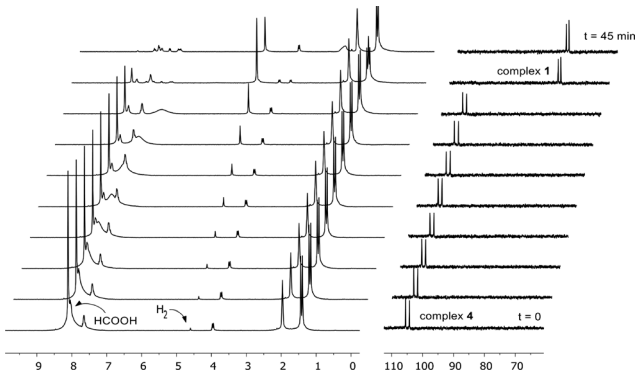

Fig. 4 Catalytic experiment (0.02 mmol of cat. **1**, 0.4 mmol of HCOOH, 2 mL of MeCN, 55 °C → 60 °C) in a 10 mm HP-NMR tube, monitored by ^{1}H NMR (left) and ^{31}P NMR spectroscopy (right) over a time-span of 45 min. The NMR spectra are stacked under an angle of 15°.

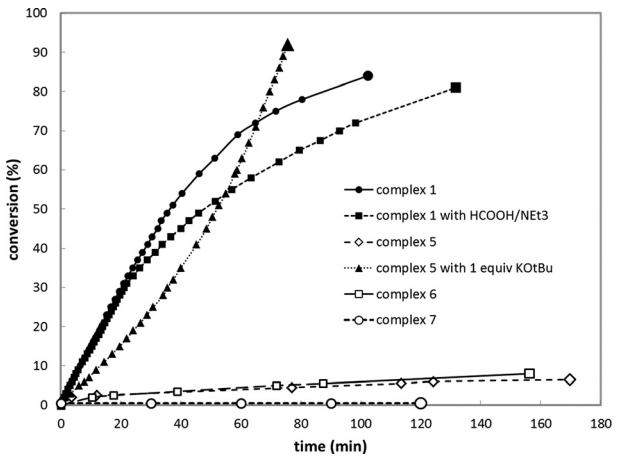

Fig. 5 Catalytic dehydrogenation curves.

of 1024). The gaseous fraction produced during reaction was analyzed by GC and no CO was found within the detection limit (δ = 10 ppm). Although the TOF achieved is still moderate under these (unoptimized) conditions, this represents the first example of base-free formic acid dehydrogenation using a Rh^{I} complex.[27]

Control experiments using complex **5** ([Rh(Cl)(CO)(PN^{H})]) bearing a bidentate PN^{H} ligand, that lacks the flanking phenyl arm (Fig. 6)[20,21] showed very low conversion in the absence of a base, likely due to blocking of the fourth coordination site by the chloride ligand. Upon addition of one equivalent of strong base to deprotonate the PN^{H} ligand, the system showed a similar TOF but a different reaction profile including significant substrate inhibition, suggesting a

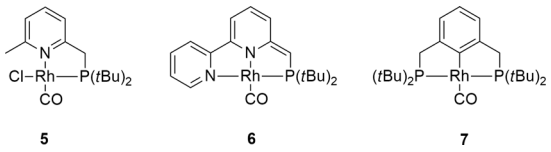

5 6 7

Fig. 6 Reference complexes that have been included in this study on Rh^{I} mediated dehydrogenation of formic acid.

different catalytic pathway for this catalyst compared to complex **1** (Fig. 4). This species likely follows a pathway involving ligand 'dearomatization'. The known Rh^{I}-pincer complexes [Rh(CO)(PNN*)] (**6**) and [Rh(CO)(PCP)] (**7**) (PNN* = 6-di(*tert*-butyl)phosphinomethine-2,2′-bipyridine; see Fig. 5)[28,29] barely exhibited activity, suggesting that low-coordinate geometries and the presence of a ligand with adaptable denticity are important.

Mechanistic considerations

Based on these catalytic results and supported by DFT calculations, two catalytic cycles are conceivable (Scheme 4). The first intramolecular path involves reversible cyclometalation as the key element. The cooperative activation of formic acid over the reactive Rh–C fragment to form formate species **4** proceeds with a moderate barrier of 17.4 kcal mol^{-1}. The transition state for a concerted hydride–proton-transfer step[30] could not be found, most likely because the hydride would be located in an unfavourable axial position (filled d_{z^2} orbital) at Rh. Alternatively, HCOOH could also oxidatively add to form a Rh^{III} intermediate that can undergo reductive elimination of the C_{Ph}–H bond. This option could not be ruled out by DFT calculations, as charged species cannot be compared to neutral species in gas phase calculations (see the ESI†). The resting state **4**, which lies −1.9 kcal mol^{-1} lower in energy than **1**, converts to monohydride **A** *via* rate-limiting β-H elimination (18.2 kcal mol^{-1} relative to **4**) concomitant with CO_2 release. Subsequent C–H oxidative addition *via* the Rh^{I}(C–H) agostic species **B** (a close analogue of a previously isolated cationic derivative[19]) and facile release of H_2 from Rh^{III}

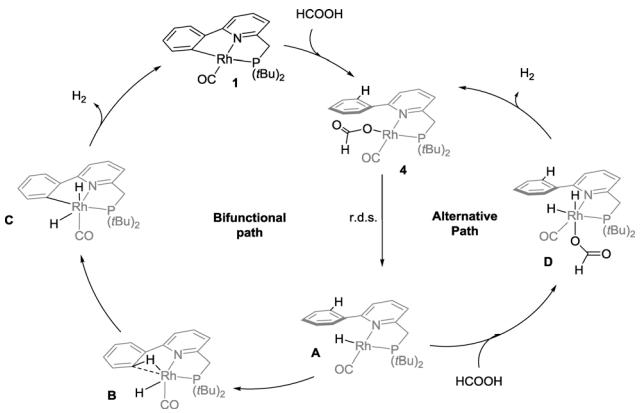

Scheme 4 Proposed mechanism for the base-free cooperative dehydrogenation of formic acid using **1** as catalyst. The DFT calculated values for the relative transition state barriers are shown in kcal mol^{-1}.

intermediate **C** regenerate **1** as the active catalyst. The reversible C–H metalation pathway, providing a hemilabile aryl moiety, is also proposed to stabilize the Rh-species between turnovers.

A second, non-cooperative path has very similar reaction barriers and shares the same rate-limiting step (from **4** to **A**), followed by oxidative addition of a second molecule of HCOOH to form dihydride intermediate **D**, which lies 0.8 kcal mol^{-1} higher in energy than **A**. Dihydride **D** generates H_2 *via* reductive elimination with a TS barrier of 5.3 kcal mol^{-1}. Given the near-identical overall reaction profiles (with a shared rate limiting step with a barrier of ~18 kcal mol^{-1}), both mechanisms are likely catalytically competent and thus co-exist under catalytic conditions, regenerating red species **1** during and/or after catalysis. The involvement of the cooperative path is supported by selective deuteration experiments, the isolation of an agostic C–H model complex as a relevant intermediate[19] and the spectroscopic observation of **4** in the presence of 10 equivalents of formic acid, followed by the regeneration of **1** with the conversion of HCOOH and release of H_2.

Conclusions

We have shown that reversible cyclometalation may be successfully employed as a motif for cooperative bond activation processes. Complex **1** readily reacts with thiols and activated amines, which leads to the protonation of the anionic carbon of the reactive flexidentate[31] ligand **L**. DFT calculations show that the release of dihydrogen is facile from putative monohydride complex **A**. The reaction of cyclometalated complex **1** with a small excess of formic acid results in formate adduct **4**. To demonstrate the potential of reversible cyclometalation in metal–ligand bifunctional catalysis, we have successfully employed Rh^I catalyst **1** in the base-free dehydrogenation of formic acid. Experimental observations in combination with DFT studies support the cooperative mode of action based on reversible cyclometalation as a feasible mechanism.

Experimental

General considerations

All reactions were carried out under an atmosphere of nitrogen using standard Schlenk techniques. The reagents were purchased from commercial suppliers and used without further purification. THF, pentane, hexane and Et_2O were distilled from sodium benzophenone ketyl. CH_2Cl_2 was distilled from CaH_2, and toluene from sodium under nitrogen. The NMR spectra (^1H, $^1H\{^{31}P\}$, ^{31}P, $^{31}P\{^1H\}$, ^{31}P-^1H and $^{13}C\{^1H\}$) were measured on a Bruker DRX 500, Bruker AV 400, Bruker DRX 300 or on a Bruker AV 300 spectrometer. The IR spectra (ATR mode) were recorded with a Bruker Alpha-p FT-IR spectrometer. The high-resolution mass spectra were recorded on a JMS-T100GCV mass spectrometer using field desorption (FD).

Complex 2, $Rh_2(SCH_2CH_2CH_2S)(CO)_2(\kappa^1\text{-}P\text{-}\mathbf{1}^H)_2$

To a solution of **1** (10 mg, 23 μmol) in CH_2Cl_2 (1 mL) was added 1,3-propanedithiol (1.1 μL, 23 μmol), resulting in an immediate color change from red to dark yellow. The solvent was evaporated to yield **2** in quantitative yield (11 mg). ^1H NMR (300 MHz, 298 K, CD_2Cl_2, ppm): δ 8.44 (d, J = 6.3 Hz, 2H), 8.14–8.07 (m, 4H), 7.63–7.40 (m, 10H), 4.21–3.82 (m, 4H, CH_2P), 2.95–2.69 (m, 4H), 2.42–2.30 (m, 2H), 1.53 (d, $^3J_{PH}$ = 12.7 Hz, 18H, P*t*Bu_2), 1.41 (d, $^3J_{PH}$ = 12.9 Hz, 18H, P*t*Bu_2). ^{31}P NMR (121 MHz, 298 K, CD_2Cl_2, ppm): δ 69.75 (d, $^1J_{RhP}$ = 151.7 Hz). ^{13}C NMR (75 MHz, 298 K, CD_2Cl_2, ppm): δ 190.58 (dd, J_{RhC} = 73.4 Hz, J_{CP} = 14.9 Hz, CO), 157.28 (s, Py-C), 155.81 (s, Py-C), 139.48 (s, Ph-C), 136.22 (s, Py-CH), 128.71 (s, Ph-CH), 128.58 (s, 2C, Ph-CH), 126.75 (s, 2C, Ph-CH), 124.71 (d, J = 2.8 Hz, Py-CH), 117.89 (s, Py-CH), 38.67 (s, SCH_2CH_2), 37.31 (d, J = 16.2 Hz, P*C*$(CH_3)_3$), 36.93 (dd, J = 15.7, 1.3 Hz, CH_2P), 31.71 (d, J = 13.0 Hz, S*C*H_2CH_2), 30.16 (dd, J = 17.4, 3.8 Hz, PC(*C*$H_3)_3$). IR (ATR, cm^{-1}): ν_{CO} 1938. HRMS (FD): m/z calcd for $C_{44}H_{62}N_2OP_2Rh_2S_2$: 966.18888 $[M–CO]^+$; found: 966.18386.

Complex 3, $Rh(NHSO_2CF_3)(CO)(\kappa^2\text{-}P,N\text{-}\mathbf{1}^H)$

To a solution of **1** (12 mg, 27 μmol) in CH_2Cl_2 (1 mL) was added trifluoromethylsulfonamide (4 mg, 27 μmol), resulting in a color change from red to orange within 5 min at room temperature. The solvent was evaporated to yield **3** in quantitative yield (16 mg). ^1H NMR (300 MHz, 298 K, CD_2Cl_2, ppm): δ 8.20–8.12 (m, 2H, Ph), 7.90 (t, J = 7.8 Hz, 1H, Py), 7.68–7.59 (m, 3H, Ph), 7.52 (t, J = 8.3 Hz, 2H, Py), 3.75 (d, $^2J_{PH}$ = 9.3 Hz, 2H, CH_2P), 1.41 (d, $^3J_{PH}$ = 14.1 Hz, 18H, P*t*Bu_2), 1.14 (s, 1H, NH). ^{31}P NMR (121 MHz, 298 K, CD_2Cl_2, ppm): δ 103.70 (d, $^1J_{RhP}$ = 152.0 Hz). ^{19}F NMR (282 MHz, 298 K, CD_2Cl_2, ppm): δ −78.68. ^{13}C NMR (75 MHz, 298 K, CD_2Cl_2, ppm): δ 189.59 (dd, J_{RhC} = 75.5 Hz, J_{CP} = 17.7 Hz, CO), 161.58 (s, Py-C), 161.50 (dd, J = 4.7, 1.8 Hz, Py-C), 139.03 (s, Py-CH and Ph-C), 130.57 (s, Ph-CH), 128.62 (s, Ph-CH), 128.52 (s, Ph-CH), 124.17 (s, Py-CH), 121.48 (d, J = 9.2 Hz, Py-CH), 120.88 (q, J_{CF} = 325.5 Hz, CF_3), 35.32 (dd, J = 20.8, 2.3 Hz, CH_2P), 34.78 (d, J = 20.1 Hz, P*C*$(CH_3)_3$), 28.92 (d, J = 4.2 Hz, PC(*C*$H_3)_3$). IR (ATR, cm^{-1}): ν_{CO} 1973. HRMS (FD): m/z calcd for $C_{22}H_{30}F_3N_2O_3PRhS$: 593.07219 $[M]^+$; found: 593.07219.

Complex 4, $Rh(OCH(O)(CO)(\kappa^2\text{-}P,N\text{-}\mathbf{1}^H))$

To a solution of **1** (4.4 mg, 10 μmol) in $CDCl_3$ (0.6 mL) was added formic acid (9.2 mg, 200 μmol), resulting in an immediate color change from red to yellow at room temperature. Due to its unstable nature, this species was only characterized *in situ* using NMR spectroscopy. ^1H NMR (400 MHz, 298 K, $CDCl_3$, ppm): δ 8.01–7.94 (m, 2H, *o*-Ph), 7.82 (ddd, J = 7.8, 7.8, 1.0 Hz, 1H, Py), 7.57–7.39 (m, 5H, 2Py, *m*-Ph, *p*-Ph), 3.73 (d, $^2J_{PH}$ = 9.6 Hz, 2H, CH_2P), 1.38 (d, $^3J_{PH}$ = 14.3 Hz, 18H, P*t*Bu_2). ^{31}P NMR (162 MHz, 298 K, $CDCl_3$, ppm): δ 105.29 (d, $^1J_{RhP}$ = 166.8 Hz).

Complex 6, Rh(Cl)(CO)(κ²-*P*,*N*-2-methyl-6-((di-*tert*-butylphosphino)-methyl)pyridine))

To a solution of 2-methyl-6-((di-*tert*-butylphosphino)methyl)-pyridine (0.025 g, 0.010 mmol) in CH_2Cl_2 (0.5 mL) was added a solution of $[Rh(CO)_2(\mu\text{-}Cl)]_2$ (0.019 g, 0.005 mmol) in CH_2Cl_2 (2 mL) and the reaction mixture was stirred overnight. After evaporation of the solvent, the product was washed with pentane (1 mL), yielding the desired complex as yellow powder (0.038 g, 0.092 mmol, 92%). ^{1}H NMR (300 MHz, 298 K, acetone-d_6, ppm): δ 7.77 (virtual t, J = 7.7 Hz, 1H, Py), 7.46 (d, J = 7.7 Hz, 1H, Py), 7.23 (d, J = 7.7 Hz, 1H, Py), 3.93 (d, $^2J_{PH}$ = 9.6 Hz, 2H, CH_2P), 3.10 (s, 3H, Py–CH_3), 1.32 (d, $^3J_{PH}$ = 13.9 Hz, 18H, P*t*Bu$_2$). ^{31}P NMR (121 MHz, 298 K, $CDCl_3$, ppm): δ 106.12 (d, $^1J_{RhP}$ = 165.0 Hz). ^{13}C NMR (75 MHz, 298 K, acetone-d_6, ppm): δ 191.85 (dd, $^1J_{RhC}$ = 73.4, $^2J_{CP}$ = 14.5 Hz, CO), 163.78 (s, Py–C), 162.52 (d, J = 3.9 Hz, Py–C), 139.74 (s, Py–CH), 124.56 (Py–CH), 121.46 (d, J = 9.0 Hz, Py–CH), 36.05 (dd, $^1J_{CP}$ = 20.3 Hz, $^2J_{RhC}$ = 2.3 Hz, CH_2P), 35.42 (d, $^1J_{CP}$ = 20.7 Hz, P*C*(CH$_3$)$_3$), 29.48 (d, $^2J_{CP}$ = 4.5 Hz, PC(*C*H$_3$)$_3$), 28.19 (s, Py–CH_3). IR (ATR, cm^{-1}): ν_{CO} 1958. HRMS(FD): *m*/*z* calcd $C_{16}H_{26}ClNOPRh$: 417.04956 $[M]^+$; found: 417.04984.

Catalytic dehydrogenation experiments

In a typical experiment, compound **1** (10 μmol) was added to the solvent (1 mL) in a 5 mL Schlenk tube equipped with a condenser and connected to a water replacement set-up. The reaction mixture was heated to the desired temperature (*e.g.* 75 °C) and stirred for 10 minutes. Formic acid (75 μL, 2 mmol) or the azeotrope HCOOH/NEt_3 (187 μL, 2 mmol HCOOH) was added to the reaction mixture and the evolved gas was collected. In the case of complex $[RhCl(CO)(PN^HP)]$, one equivalent of potassium *tert*-butoxide in THF (1 M) was added at r.t. to abstract the chloride ligand. After stirring this mixture for 5 min, 75 μL HCOOH was added. The mixture was rapidly heated to 75 °C and the evolved gas was collected. The set-up was calibrated with a Brooks flow meter type 1054-3C and the evolved gases were analyzed with a G·A·S Compact GC (Rt-MSieve 5A 20 m × 0.32 mm + Rt-Q-bond 2 m × 0.32 mm).

X-ray crystal structure determination of complex 2

$C_{45}H_{62}N_2O_2P_2RhS_2$, F_w = 994.85, yellow block, 0.25 × 0.19 × 0.09 mm^3, monoclinic, $P2_1/n$ (no. 14), a = 12.7487(4), b = 19.7725(6), c = 18.4361(5) Å, β = 103.046(1)°, V = 4527.3(2) Å^3, Z = 4, D_x = 1.460 g cm^{-3}, μ = 0.93 mm^{-1}. 60 826 reflections were measured on a Bruker Kappa ApexII diffractometer with a sealed tube and a Triumph monochromator (λ = 0.71073 Å) at a temperature of 150(2) K up to a resolution of $(\sin\theta/\lambda)_{max}$ = 0.65 Å^{-1}. The X-ray intensities were measured on a Bruker Kappa ApexII diffractometer with a sealed tube and a Triumph monochromator (λ = 0.71073 Å) at a temperature of 150(2) K. The intensities were integrated with the Eval15 software.[32] Multi-scan absorption correction and scaling was performed with SADABS[33] (correction range 0.67–0.75). 10 392 reflections were unique (R_{int} = 0.039), of which 8330 were observed [$I > 2\sigma(I)$]. The structure was solved with Patterson superposition methods using SHELXT.[34] Least-squares refinement was performed with SHELXL-97 (ref. 35) against F^2 of all reflections. Non-hydrogen atoms were refined freely with anisotropic displacement parameters. All hydrogen atoms were located in difference Fourier maps and refined using a riding model. 508 parameters were refined with no restraints. R_1/wR_2 [$I > 2\sigma(I)$]: 0.0255/0.0542. R_1/wR_2 [all refl.]: 0.0396/0.0580. S = 1.023. Residual electron density between −0.32 and 0.32 e Å^{-3}. CCDC 1422009 contains the supplementary crystallographic data for this paper.

DFT calculations

Geometry optimizations were carried out with the Turbomole program package[36] coupled to the PQS Baker optimizer[37] *via* the BOpt package,[38] at the ri-DFT level using the BP86 (ref. 39) functional and the resolution-of-identity (ri) method.[40] We optimized the geometries of all stationary points at the def2-TZVP basis set level,[41] using Grimme's dispersion corrections (disp3 version)[42] and a tight energy grid (m5). The identity of the transition states was confirmed by following the imaginary frequency in both directions (IRC). All minima (no imaginary frequencies) and transition states (one imaginary frequency) were characterized by calculating the Hessian matrix. ZPE and gas-phase thermal corrections (entropy and enthalpy, 298 K, 1 bar) from these analyses were calculated using standard thermodynamics.

Acknowledgements

This work was funded by the European Research Council (ERC, Starting Grant 279097, EuReCat to J. I. v. d. V.). We thank Sander Oldenhof for useful discussions and practical tips on FA dehydrogenation chemistry, Ed Zuidinga for MS measurements and Christophe Rebreyend and Sandra de Boer for supplying compounds **7** and **8**, respectively. The X-ray diffractometer at Utrecht University was funded by NWO.

Notes and references

1 Reviews: D. L. J. Broere, R. Plessius and J. I. van der Vlugt, *Chem. Soc. Rev.*, 2015, **44**, 6886–6915; D. Milstein, *Philos. Trans. R. Soc., A*, 2015, **373**, 20140189; O. R. Luca and R. H. Crabtree, *Chem. Soc. Rev.*, 2013, **42**, 1440–1459; J. I. van der Vlugt, *Eur. J. Inorg. Chem.*, 2012, 363–375; V. Lyaskovskyy and B. de Bruin, *ACS Catal.*, 2012, **2**, 270–279; T. Ikariya, *Top. Organomet. Chem.*, 2011, **37**, 31–54; D. Milstein, *Top. Catal.*, 2010, **53**, 915–923.

2 Reviews: J. I. van der Vlugt and J. N. H. Reek, *Angew. Chem., Int. Ed.*, 2009, **48**, 8832–8846; C. Gunanathan and D. Milstein, *Acc. Chem. Res.*, 2011, **44**, 588–602; C. Gunanathan and D. Milstein, *Chem. Rev.*, 2014, **114**, 12024–12087; J. R. Khusnutdinova and D. Milstein, *Angew. Chem., Int. Ed.*, 2015, **54**, 12236–12273.

3 H. Li, B. Zheng and K.-W. Huang, *Coord. Chem. Rev.*, 2015, **293–294**, 116–138; B. Bichler, C. Holzhacker, B. Stöger,

M. Puchberger, L. F. Veiros and K. Kirchner, *Organometallics*, 2013, **32**, 4114–4121; D. Benito-Garagorri and K. Kirchner, *Acc. Chem. Res.*, 2008, **41**, 201–213.

4 Overview: W.-H. Wang, J. T. Muckerman, E. Fujita and Y. Himeda, *New J. Chem.*, 2013, **37**, 1860–1866; See also: C. M. Moore and N. K. Szymczak, *Chem. Commun.*, 2013, **49**, 400–402; J. F. Hull, Y. Himeda, W.-H. Wang, B. Hashiguchi, R. Periana, D. J. Szalda, J. T. Muckerman and E. Fujita, *Nat. Chem.*, 2012, **4**, 383–388; R. Kawahara, K. Fujita and R. Yamaguchi, *Angew. Chem., Int. Ed.*, 2012, **51**, 12790–12794.

5 Reviews: B. Zhao, Z. Han and K. Ding, *Angew. Chem., Int. Ed.*, 2013, **52**, 4744–4788; S. Schneider, J. Meiners and B. Askevold, *Eur. J. Inorg. Chem.*, 2012, 412–429; S. Kuwata and T. Ikariya, *Dalton Trans.*, 2010, **39**, 2984–2992.

6 Rh^{III}: J. R. Krumper, M. Gerisch, A. Magistrato, U. Rothlisberger, R. G. Bergman and T. D. Tilley, *J. Am. Chem. Soc.*, 2004, **126**, 12492–12502.

7 Ir^{III}: Y. Gloaguen, L. M. Jongens, M. Lutz, J. N. H. Reek, B. de Bruin and J. I. van der Vlugt, *Organometallics*, 2013, **32**, 4284–4291; F. Morandini, B. Longato and S. Bresadola, *J. Organomet. Chem.*, 1977, **132**, 291–299; J. A. Raskatov, S. Spiess, C. Gnamm, K. Brödner, F. Rominger and G. Helmchen, *Chem. – Eur. J.*, 2010, **16**, 6601–6615; Pt^{II} (and Ir^{III}): S. Musa, R. Romm, C. Azerraf, S. Kozuch and D. Gelman, *Dalton Trans.*, 2011, **40**, 8760–8763; Au^{III}: D. A. Smith, D.-A. Roşca and M. Bochmann, *Organometallics*, 2012, **31**, 5998–6000; Pd^{II}: A. D. Getty and K. I. Goldberg, *Organometallics*, 2001, **20**, 2545–2551; Ru^{II}: J. Becker, T. Modl and V. H. Gessner, *Chem. – Eur. J.*, 2014, **20**, 11295–11299; Ni^{II}: D. V. Gutsulyak, W. E. Piers, J. Borau-Garcia and M. Parvez, *J. Am. Chem. Soc.*, 2013, **135**, 11776–11779.

8 Roll-over complexes: L. Maidich, G. Zuri, S. Stoccoro, M. A. Cinellu, M. Masia, A. Zucca and U. Sassari, *Organometallics*, 2013, **32**, 438–448; B. Butschke and H. Schwarz, *Chem. Sci.*, 2012, **3**, 308–326; J. Kwak, Y. Ohk, Y. Jung and S. Chang, *J. Am. Chem. Soc.*, 2012, **134**, 17778–17788; A. Zucca, G. L. Petretto, M. L. Cabras, S. Stoccoro, M. A. Cinellu, M. Manassero and G. Minghetti, *J. Organomet. Chem.*, 2009, **694**, 3753–3761.

9 G. Choi, H. Tsurugi and K. Mashima, *J. Am. Chem. Soc.*, 2013, **135**, 13149–13161.

10 L. Taghizadeh Ghoochany, C. Kerner, S. Farsadpour, F. Menges, Y. Sun, G. Niedner-Schatteburg and W. R. Thiel, *Eur. J. Inorg. Chem.*, 2013, 4305–4317.

11 K. Ghatak, M. Mane and K. Vanka, *ACS Catal.*, 2013, **3**, 920–927.

12 C. Boulho and J.-P. Djukic, *Dalton Trans.*, 2010, **39**, 8883–8905.

13 P. Bhattacharya, J. A. Krause and H. Guan, *J. Am. Chem. Soc.*, 2014, **136**, 11153–11161.

14 Selected recent examples: R. Tanaka, M. Yamashita, L. W. Chung, K. Morokuma and K. Nozaki, *Organometallics*, 2011, **30**, 6742–6750; E. A. Bielinski, P. O. Lagaditis, Y. Zhang, B. Q. Mercado, C. Würtele, W. H. Bernskoetter, N. Hazari and S. Schneider, *J. Am. Chem. Soc.*, 2014, **136**, 10234–10237; G. A. Filonenko, R. van Putten, E. N. Schulpen, E. J. M. Hensen and E. A. Pidko, *ChemCatChem*, 2014, **6**, 1526–1530.

15 B. Loges, A. Boddien, H. Junge and M. Beller, *Angew. Chem., Int. Ed.*, 2008, **47**, 3962–3965; S. Enthaler, J. von Langermann and T. Schmidt, *Energy Environ. Sci.*, 2010, **3**, 1207–1217; A. Boddien, C. Federsel, P. Sponholz, D. Mellmann, R. Jackstell, H. Junge, G. Laurenczy and M. Beller, *Energy Environ. Sci.*, 2012, **5**, 8907–8911.

16 Y. Gao, J. Kuncheria, R. J. Puddephatt and G. P. A. Yap, *Chem. Commun.*, 1998, 2365–2366; A. Boddien, D. Mellmann, F. Gärtner, R. Jackstell, H. Junge, P. J. Dyson, G. Laurenczy, R. Ludwig and M. Beller, *Science*, 2011, **333**, 1733–1736; J. F. Hull, Y. Himeda, W.-H. Wang, B. Hashiguchi, R. Periana, D. J. Szalda, J. T. Muckerman and E. Fujita, *Nat. Chem.*, 2012, **4**, 383–388; J. H. Barnard, C. Wang, N. G. Berry and J. Xiao, *Chem. Sci.*, 2013, **4**, 1234–1244; R. E. Rodríguez-Lugo, M. Trincado, M. Vogt, F. Tewes, G. Santiso-Quinones and H. Grützmacher, *Nat. Chem.*, 2013, **5**, 342–347; S. Oldenhof, B. de Bruin, M. Lutz, M. A. Siegler, F. W. Patureau, J. I. van der Vlugt and J. N. H. Reek, *Chem. – Eur. J.*, 2013, **19**, 11507–11511; W.-H. Wang, S. Xu, Y. Manaka, Y. Suna, H. Kambayashi, J. T. Muckerman, E. Fujita and Y. Himeda, *ChemSusChem*, 2014, **7**, 1976–1983; T. W. Myers and L. A. Berben, *Chem. Sci.*, 2014, **5**, 2771–2777; F. Bertini, I. Mellone, A. Ienco, M. Peruzzine and L. Gonsalvi, *ACS Catal.*, 2015, **5**, 1254–1265; J. Kethandaraman, M. Czaun, A. Goeppert, R. Haiges, J. P. Jones, R. B. May, G. K. S. Prakash and G. A. Olah, *ChemSusChem*, 2015, **8**, 1442–1451.

17 J. I. van der Vlugt, M. Lutz, E. A. Pidko, D. Vogt and A. L. Spek, *Dalton Trans.*, 2009, 1016–1023; J. I. van der Vlugt, M. A. Siegler, M. Janssen, D. Vogt and A. L. Spek, *Organometallics*, 2009, **28**, 7025–7032; R. C. Bauer, Y. Gloaguen, M. Lutz, J. N. H. Reek, B. de Bruin and J. I. van der Vlugt, *Dalton Trans.*, 2011, **40**, 8822–8829; Y. Gloaguen, W. Jacobs, B. de Bruin, M. Lutz and J. I. van der Vlugt, *Inorg. Chem.*, 2013, **52**, 1682–1684; F. G. Terrade, M. Lutz, J. I. van der Vlugt and J. N. H. Reek, *Eur. J. Inorg. Chem.*, 2014, 1826–1835; D. L. J. Broere, B. de Bruin, J. N. H. Reek, M. Lutz, S. Dechert and J. I. van der Vlugt, *J. Am. Chem. Soc.*, 2014, **136**, 11574–11577; S. Oldenhof, F. G. Terrade, M. Lutz, J. I. van der Vlugt and J. N. H. Reek, *Organometallics*, 2015, **34**, 3209–3215; D. L. J. Broere, L. L. Metz, B. de Bruin, J. N. H. Reek, M. A. Siegler and J. I. van der Vlugt, *Angew. Chem., Int. Ed.*, 2015, **54**, 1516–1520; V. Vreeken, M. A. Siegler, B. de Bruin, J. N. H. Reek, M. Lutz and J. I. van der Vlugt, *Angew. Chem., Int. Ed.*, 2015, **54**, 7055–7059; Z. Tang, E. Otten, J. N. H. Reek, J. I. van der Vlugt and B. de Bruin, *Chem. – Eur. J.*, 2015, **21**, 12683–12693; S. Oldenhof, M. Lutz, J. I. van der Vlugt and J. N. H. Reek, *Chem. Commun.*, 2015, **51**, 15200–15203.

18 M. Brookhart and M. L. H. Green, *J. Organomet. Chem.*, 1983, **250**, 395–408; M. Brookhart, M. L. H. Green and G. Parkin, *Proc. Natl. Acad. Sci. U. S. A.*, 2007, **104**, 6908–6914.8.

19 L. S. Jongbloed, B. de Bruin, J. N. H. Reek, M. Lutz and J. I. van der Vlugt, *Chem. – Eur. J.*, 2015, **21**, 7297–7305.

20 S. Y. de Boer, Y. Gloaguen, M. Lutz and J. I. van der Vlugt, *Inorg. Chim. Acta*, 2012, **380**, 336–342.
21 S. Y. de Boer, Y. Gloaguen, J. N. H. Reek, M. Lutz and J. I. van der Vlugt, *Dalton Trans.*, 2012, **41**, 11276–11283.
22 J. I. van der Vlugt, M. Lutz, E. A. Pidko, D. Vogt and A. L. Spek, *Dalton Trans.*, 2009, 1016–1023.
23 J. I. van der Vlugt, E. A. Pidko, R. C. Bauer, Y. Gloaguen, M. K. Rong and M. Lutz, *Chem. – Eur. J.*, 2011, **17**, 3850–3854.
24 M. A. F. Hernandez-Gruel, G. Gracia-Arruego, A. B. Rivas, I. T. Dobrinovitch, F. J. Lahoz, A. J. Pardey, L. A. Oro and J. J. Pérez-Torrente, *Eur. J. Inorg. Chem.*, 2007, 5677–5683; F. Monteil, R. Queau and P. Kalck, *J. Organomet. Chem.*, 1994, **480**, 177–184; W. D. Jones, J. Garcia and H. Torrens, *Acta Crystallogr., Sect. E: Struct. Rep. Online*, 2005, **61**, m2204–m2206.
25 Notably, the reaction of **1** with thiophenol gave different spectral features, with a doublet at 99 ppm ($^1J_{Rh-P}$ = 136.3 Hz) in MeCN-d_3. When C_6D_6 was used as solvent, two species with similar shifts and coupling constants to complex **2** were observed, *i.e.* doublets at 66 ppm ($^1J_{Rh-P}$ = 152.1 Hz) and 72 ppm ($^1J_{Rh-P}$ = 152.9 Hz). The species interconvert when the solvent is changed in the same sample. These results indicate that monomeric complexes are formed when polar solvents are used in the reaction, but no conclusive structural evidence could be obtained.
26 The catalytic dehydrogenation of formic acid is not faster when the azeotrope HCOOH/Et_3N 5:2 is used, but the TOF can be increased as more equivalents of the azeotrope are added under the same conditions. Increasing the formic acid concentration without a base results in a loss of activity, presumably because dormant species **5** is formed at too high concentrations of acid.
27 Formate decomposition: E. N. Yurchenko and N. P. Anikeenko, *React. Kinet. Catal. Lett.*, 1975, **2**, 65–72; CO_2 hydrogenation: J.-C. Tsai and K. M. Nicholas, *J. Am. Chem. Soc.*, 1992, **114**, 5117–5124.
28 Y. Gloaguen, C. Rebreyend, M. Lutz, P. Kumar, M. I. Huber, J. I. van der Vlugt, S. Schneider and B. de Bruin, *Angew. Chem., Int. Ed.*, 2014, **53**, 6814–6818.
29 K.-W. Huang, D. C. Grills, J. H. Han, D. J. Szalda and E. Fujita, *Inorg. Chim. Acta*, 2008, **361**, 3327–3331.
30 S. Oldenhof, M. Lutz, B. de Bruin, J. I. van der Vlugt and J. N. H. Reek, *Chem. Sci.*, 2015, **6**, 1027–1034; See also: S. Oldenhof, J. I. van der Vlugt and J. N. H. Reek, *Catal. Sci. Technol.*, 2015, DOI: 10.1039/C5CY01476J.
31 R. Lindner, B. van den Bosch, M. Lutz, J. N. H. Reek and J. I. van der Vlugt, *Organometallics*, 2011, **30**, 499–510.
32 A. M. M. Schreurs, X. Xian and L. M. J. Kroon-Batenburg, *J. Appl. Crystallogr.*, 2010, **43**, 70–82.
33 G. M. Sheldrick, *SADABS*, Universität Göttingen, Germany, 2008.
34 G. M. Sheldrick, *Acta Crystallogr., Sect. A: Found. Adv.*, 2015, **71**, 1–8.
35 G. M. Sheldrick, *Acta Crystallogr., Sect. A: Found. Adv.*, 2008, **64**, 112–122.
36 R. Ahlrichs, *Turbomole Version 6.5*, Theoretical Chemistry Group, University of Karlsruhe, 2013.
37 Parallel Quantum Solutions, *PQS version 2.4*, Fayetteville, Arkansas (USA), 2001; The Baker optimizer is available separately from PQS upon request: I. Baker, *J. Comput. Chem.*, 1986, **7**, 385–395.
38 P. H. M. Budzelaar, *J. Comput. Chem.*, 2007, **28**, 2226–2236.
39 A. D. Becke, *Phys. Rev. A: At., Mol., Opt. Phys.*, 1988, **38**, 3098–3100; J. P. Perdew, *Phys. Rev. B: Condens. Matter Mater. Phys.*, 1986, **33**, 8822–8824.
40 M. Sierka, A. Hogekamp and R. Ahlrichs, *J. Chem. Phys.*, 2003, **118**, 9136–9148.
41 A. Schäfer, H. Horn and R. Ahlrichs, *J. Chem. Phys.*, 1992, **97**, 2571–2577.
42 S. Grimme, J. Antony, S. Ehrlich and H. Krieg, *J. Chem. Phys.*, 2010, **132**, 154104–154119.